Combined effect of confinement and dielectric exclusion on ion adsorption in slits, pores, and cavities

Cite as: AIP Advances 14, 125323 (2024); doi: 10.1063/5.0237169
Submitted: 3 September 2024 • Accepted: 5 December 2024 •
Published Online: 24 December 2024

János Szarvas,[1] Mónika Valiskó,[1] Dirk Gillespie,[2] and Dezső Boda[1,a)]

AFFILIATIONS

[1] Center for Natural Sciences, University of Pannonia, Egyetem u. 10, Veszprém 8200, Hungary
[2] Department of Physiology and Biophysics, Rush University Medical Center, Chicago, Illinois 60612, USA

[a)] **Author to whom correspondence should be addressed:** boda.dezso@mk.uni-pannon.hu

ABSTRACT

We present simulation results for the Donnan equilibrium between a homogeneous bulk reservoir and inhomogeneous confining geometries with varying number of restricted dimensions, d_c. Planar slits ($d_c = 1$), cylindrical pores ($d_c = 2$), and spherical cavities ($d_c = 3$) are considered. The walls have a negative surface charge density. Because different dielectric constants are used in the reservoir and confined system, we used the Donnan grand canonical Monte Carlo method [Boda and Gillespie, J. Mol. Liq. **391**, 123372 (2023)] to simulate the equilibrium. The systems with larger confining dimensionality produce greater adsorption of counterions (cations) into the confinements, so cation selectivity increases with increasing dimensionality. The systems with smaller dielectric constants produce more effective coion (anion) exclusion, so cation selectivity increases with decreasing dielectric constant. The combined effect of a more confining space and solvation penalty produces even more efficient anion exclusion and cation selectivity than each separately.

I. INTRODUCTION

The basic question of partition equilibria is how a component distributes between two subsystems (e.g., two immiscible liquid phases) when it can move between them. The condition for chemical equilibrium is the equality of the chemical potentials of the component in the two subsystems. For example, with a semipermeable membrane, the component that can permeate the membrane can be the solvent (osmosis) or an ionic component, as in the case of the cell membrane where the membrane is permeable for K^+ ions.

The distribution of charged particles and ions among different media is a fundamental phenomenon. There are many examples, ranging from energy storage (e.g., supercapacitors[1]) to nanotechnology (energy conversion[2] and water purification[3]) to biology (e.g., calcium microdomains in cell,[4] cavities and binding sites within macromolecules,[5–7] and function of ion channels across cell membranes[8,9]). A fundamental question in ion partitioning is how many ions are adsorbed from a bulk-phase electrolyte into environments with properties that are different from those of the bulk phase.

One important aspect of this is the role of ion confinement in these systems. All of them work because they confine ions to some extent, ranging from sub-nanometer tubes (e.g., ion channels) and cavities (e.g., macromolecular binding sites) up to multi-nanometer and larger porous materials (e.g., supercapacitors and desalination membranes). In all these systems (especially the engineered ones), it is not clear what the optimal confining geometry (e.g., cavity, cylinder, or slit) is or what its optimal size should be. Changing any of these will result in secondary changes, like the effective dielectric environment seen by the ions; smaller, more confining geometries will reduce the mobility of water molecules. Therefore, while all these systems are qualitatively different in many ways, they also share a number of traits that are fundamental to how they work and how they might be optimized.

In order to define how these primary and secondary changes affect ion adsorption, one could study each system separately. The

approach we choose instead is to abstract these systems down to the fundamental building blocks they have in common and study the changes over a broad parameter space. This necessarily requires substantial simplifications and idealizations. In return, however, we hope to identify general physical principles that will place each specific system into a much broader context. As single points within a new broad landscape, each system can then potentially be optimized by following the guidelines the underlying general physics suggests.

The goal of this study is to use computational modeling to investigate how the ions of an electrolyte are distributed between a homogeneous bulk-phase solution and an inhomogeneous confined system. Beyond geometric confinement, an additional difference between the two subsystems is that the dielectric constants may be different in the two systems.

The dielectric constant characterizes the ability of a medium to screen the charge of an ion, or, conversely, the ability of an ion to polarize the medium. Dielectrics may differ for a number of reasons. For example, the solvent may be different in the two liquid phases. The same solvent may also change its screening ability when placed in an electric field (dielectric saturation). This electric field may be due to the charges of the functional groups on the surfaces, the charges of the electrodes, or the presence of ions themselves. For example, the dielectric constant is lower in a concentrated electrolyte solution than in a dilute electrolyte.[10–12]

Spatial confinement can also affect the behavior of liquids,[12–15] and hence the dielectric constant,[16] as shown by theoretical[17] and molecular dynamics[18–22] studies. The difference in the dielectric environment between bulk systems and porous membranes has been the focus of experimental and modeling studies on the dielectric exclusion of ions, salt partitioning, and nanofiltration.[23–30]

In this study, by spatial confinement, we mean narrow pores, slits, or cavities, where the electrolyte is surrounded by charged walls. Depending on how these charged walls are curved and on the symmetry of the system, we distinguish different geometries and define the dimensionality of the system as the number of dimensions in which the ions are restricted (d_c, see Fig. 1):

Bulk: The system is homogeneous in all the three dimensions; confinement is not present ($d_c = 0$).

Slit: The electrolyte is confined in one dimension ($d_c = 1$) between two parallel infinite walls. The system is homogeneous in the two planar dimensions; it has a planar symmetry.

Pore: The electrolyte is confined in two dimensions ($d_c = 2$) inside an infinite cylinder. The system is homogeneous in the axial dimension; it has a cylindrical symmetry.

Cavity: The electrolyte is enclosed in a sphere. The system is confined in all the three dimensions ($d_c = 3$); it has a spherical symmetry.

These and similar less symmetric structures play an increasingly important role in nanotechnology and molecular biology.[31,32] The thermodynamic (statistical mechanical) properties of real porous media may be calculated as a superposition of the statistical mechanical properties of these three basic geometries.

In general, any equilibrium between two subsystems where there is some electrical asymmetry between them can be called a Donnan equilibrium. In this work, this asymmetry is caused by (1) the presence of charged walls at which electrical double layers form and (2) the difference in the dielectric screening environments in the two subsystems (i.e., the different dielectric constants).

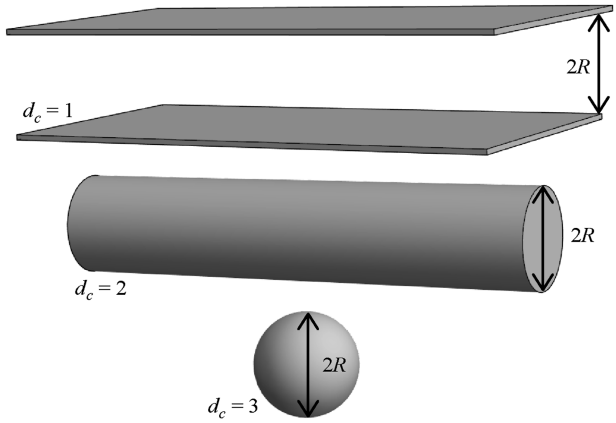

FIG. 1. Confined geometries of different dimensionalities: slit ($d_c = 1$), cylindrical pore ($d_c = 2$), and spherical cavity ($d_c = 3$). The radius of the cylindrical and spherical geometries, as well as the half width of the slit, is denoted by R.

Donnan equilibrium has been studied by numerous modeling methods.[29,33–35] The Grand Canonical Monte Carlo (GCMC) simulation method is especially well-suited for this purpose. Barr and Panagiotopoulos,[36] for example, proposed a GCMC procedure to determine the thermodynamic equilibrium of such a system. They implemented specific ion insertion/removal steps that allowed the calculation of the electrical potential difference (Donnan potential) between the two baths. A version of the method combined with a grand-reaction method at constant pH[37] simulates the ionization equilibria.

The Donnan Grand Canonical Monte Carlo (D-GCMC) method of Boda and Gillespie[38] differs from these methods by allowing the dielectric constants to be different in the two subsystems. In this case, one must include the solvation (Born) energy penalty in the chemical potential (Fig. 2). The Born energy is commonly used in studies where ions are partitioned between bulk phases and polymer membranes.[23–30]

The number of articles in the literature where two or more of the three geometries (slit, pore, and cavity) are considered is relatively limited. Sánchez-Arellano *et al.*[39] studied the electrokinetic properties of electrolytes confined in slit-like and cylindrical nanopores by the hypernetted chain/mean spherical approximation and found that the ion–ion correlations and confinement effects are enhanced in the cylindrical pore. Aguilar-Pineda *et al.*[40] studied the pressure behavior of electrolytes confined in the three geometries.

Cherstvy[41] studied the adsorption of polyelectrolytes in all the three geometries with a theoretical approach. Szymczyk and Fievet[42] studied the rejection rate of ions from nanofiltration membranes using a model that included steric effects, image forces, and dielectric exclusion for both slit-like and cylindrical pores compared to slit-like ones. They showed that the dielectric exclusion was necessary to reproduce the experimental data. Buyukdagli *et al.*[43,44] used a field theoretic variational approach to study ion exclusion phase transitions in planar and cylindrical nanopores. They considered the computationally difficult case of confining dielectrics that go

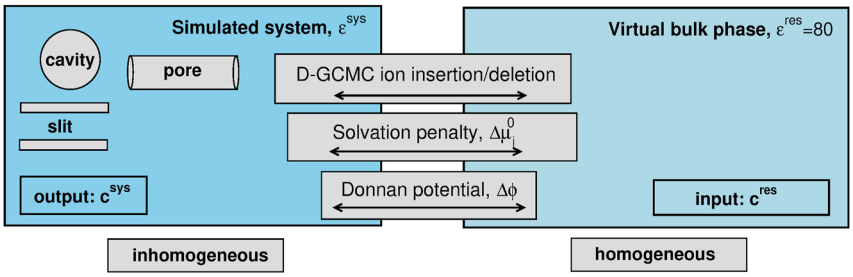

FIG. 2. Schematic drawing of the coexisting systems. Left: inhomogeneous confined system (sys) of various geometries. Right: homogeneous reservoir (res). The system is simulated with the D-GCMC method in the grand canonical ensemble, so ion insertion/deletion steps are applied. The two subsystems may have different dielectric constants, ϵ^{sys} and ϵ^{res}, so a solvation penalty, $\Delta\mu_i^0$, is applied between the two subsystems. The role of the Donnan potential, $\Delta\phi$, is to make the system charge neutral.

together with a dielectric interface and induced charges. This study has also been performed for spherical confinements.[45]

In this work, we provide a systematic analysis for the different geometries in conjunction with dielectric exclusion to show their combined effect. We find that the two together produces better counterion selectivity and coion exclusion than each alone. That is, the two effects, when working together, are more efficient than each individually.

II. MODEL AND METHOD

The condition of thermodynamic equilibrium between subsystems "sys" (the simulated confined system) and "res" (reservoir) is the equality of electrochemical potentials for ionic species i as $\mu_i^{sys} = \mu_i^{res}$, where

$$\mu_i^{sys} = \mu_i^{0,sys} + kT \ln\left(c_i^{sys}(\mathbf{r})V_0\right) + \mu_i^{ex,sys}(\mathbf{r}) + q_i\phi^{sys}, \tag{1}$$

$$\mu_i^{res} = \mu_i^{0,res} + kT \ln\left(c_i^{res}V_0\right) + \mu_i^{ex,res} + q_i\phi^{res}. \tag{2}$$

In these equations, k is Boltzmann's constant, T is the temperature, and for ion species i, q_i is the ionic charge, c_i^{sys} and c_i^{res} are the concentrations in the system and the reservoir, V_0 is a unit volume, $\mu_i^{ex,sys}$ and $\mu_i^{ex,res}$ are the excess chemical potentials due to the interactions between the ions (zero at infinite dilution), and ϕ^{sys} and ϕ^{res} are the mean electrical potentials in the respective baths. $\mu_i^{0,sys}$ and $\mu_i^{0,res}$ are self (or reference) terms that contain the solvation terms due to the interaction of the ion with the surrounding dielectric medium (solvent) undisturbed by other ions. The terms $\mu_i^{0,sys}$ and $q_i\phi^{sys}$ are present even at infinite dilution. The quantities $c_i^{sys}(\mathbf{r})$ and $\mu_i^{ex,sys}(\mathbf{r})$ are position dependent, because the system is inhomogeneous, while the reservoir is homogeneous.

From the equilibrium condition, we obtain the equalities for cations and anions (or, any additional species) that

$$\mu_i^{c,sys} + \Delta\mu_i^0 + q_i\Delta\phi = \mu_i^{c,res}, \tag{3}$$

where $\Delta\phi = \phi^{sys} - \phi^{res}$ is the Donnan potential, $\Delta\mu_i^0 = \mu_i^{0,sys} - \mu_i^{0,res}$ is the difference of the solvation free energy between the two baths, while $\mu_i^{c,sys} = kT \ln\left(c_i^{sys}V_0\right) + \mu_i^{ex,sys}$ and $\mu_i^{c,res} = kT \ln\left(c_i^{res}V_0\right) + \mu_i^{ex,res}$ are the configurational chemical potentials. The system contains two equations [Eq. (3) refers to cation and anion as well] and three unknowns (c_+^{sys}, c_-^{sys}, and $\Delta\phi$), so a third equation expressing sys charge neutrality is required,

$$\sum_i q_i \int_V c_i^{sys}(\mathbf{r})d\mathbf{r} + \sigma A = 0, \tag{4}$$

where A is the area of the confining surface. The system is solved with the D-GCMC method, in which insertions/deletions of individual ions are performed for the simulated system for spherical cavities and cylindrical pores. For the slit, we insert neutral groups of ions (ion pairs in the case 1:1 electrolytes studied here). Using Eq. (3), the acceptance criterion of the insertion/deletion steps is obtained as

$$p_{i,\chi} = \frac{N_i!(V/V_0)^\chi}{(N_i+\chi)!}\exp\left(-\frac{\Delta U - \chi\mu_i^{c,sys}}{kT}\right) = \frac{N_i!(V/V_0)^\chi}{(N_i+\chi)!} \times \exp\left(-\frac{\Delta U - \chi\left[\mu_i^{c,res} - \Delta\mu_i^0 - q_i\Delta\phi\right]}{kT}\right), \tag{5}$$

where V is the volume of sys, N_i is the number of ions of species i before insertion/deletion, $\chi = 1$ for insertion, $\chi = -1$ for deletion, and ΔU is the energy change. The following are the steps to be performed:

1. Specify the concentrations of the reservoir: $\{c_i^{res}\}$.
2. Compute the excess and configurational chemical potentials in the reservoir with the adaptive GCMC method:[46] $\{\mu_i^{c,res}\}$.
3. Use those configurational chemical potentials in the acceptance criterion of D-GCMC [Eq. (5)] and subtract the solvation penalty ($\Delta\mu_i^0$) and the interaction with the Donnan potential ($q_i\Delta\phi$). The simulation provides the concentrations in the simulated system: $\{c_i^{sys}\}$.
4. To find the $\Delta\phi$ value that provides charge neutrality [Eq. (4)], we perform several short simulations and apply linear interpolation. The Donnan potential obtained this way is used in the production run.

The ions of the electrolyte are modeled as hard spheres with point charges in their centers (the "primitive" model). The spheres

cannot overlap with each other or with the wall. The interaction potential is

$$u_{ij}(r) = \begin{cases} \infty & \text{for} \quad r < R_i + R_j, \\ \dfrac{1}{4\pi\epsilon_0\epsilon^{\text{sys}}}\dfrac{q_i q_j}{r} & \text{for} \quad r \geq R_i + R_j, \end{cases} \tag{6}$$

where R_i and R_j are the ionic radii of species i and j, ϵ_0 is the permittivity of vacuum, and r is the distance between the centers of the ions. We consider 1:1 electrolytes in this study with $R_+ = R_- = 0.15$ nm.

The solvation penalty of moving the ion from the ϵ^{res} medium to the ϵ^{sys} medium can be estimated from Born's theory[47] as

$$\Delta\mu_i^0 = \frac{q_i^2}{8\pi\epsilon_0 R_i^{\text{B}}}\left(\frac{1}{\epsilon^{\text{sys}}} - \frac{1}{\epsilon^{\text{res}}}\right), \tag{7}$$

where R_i^{B} is a parameter for which various choices can be applied. It can be the ionic radius ($R_i^{\text{B}} = R_i$), but it is well known that that choice overestimates the hydration free energy (compared to experiment). Therefore, the Born radius most often used is the one obtained from fitting Eq. (7) to the experimental hydration free energies. The Born radius is generally larger than the radius of the "bare" ion, e.g., the Pauling radius. To avoid using an additional parameter in this work, we use the choice of $R_i^{\text{B}} = R_i$, but the reader should be aware of the limitations of that choice as the limitations of the Born theory itself.[28,29]

The Born model was developed to estimate the solvation penalty of bringing an ion from one dielectric bulk medium to another. Here, we assume that the penalty scales similarly for moving an ion into a low-dielectric confining geometry. A more nuanced approach of having a location and concentration dependent dielectric is computationally too expensive in our simulations here with curved dielectric interfaces.[48] In that case, explicit dielectric interfaces would be present in the simulation cell with the computationally challenging case of ions passing through the interface.[49] The advantage of the present approach is that the two subsystems are not part of the same simulation cell; they are only connected by the chemical potential.

We end with a sketch of a proof that the Donnan potential $\Delta\phi$ is a uniquely defined number (i.e., not location dependent), even for an inhomogeneous system. By combining Eqs. (1) and (2), one can solve for $q_i c_i^{\text{sys}}(\mathbf{r})$. Formally integrating this over $\mathbf{r}$, summing over i, and equating this to $-\sigma A$ (i.e., applying the total charge neutrality), one gets a polynomial of the form[50]

$$f(x) = sx^{q_N} + \sum_{i=1}^{N-1} q_i a_i x^{q_N - q_i} + q_N a_N, \tag{8}$$

where $x = e^{\Delta\phi}$, the valences $q_1, \ldots, q_N$ are ordered from smallest to largest, $a_i > 0$ is the ratio of the integrated $c_i^{\text{sys}}(\mathbf{r})$ with $e^{-q_i\Delta\phi}$ taken out of the integral to $|\sigma A|$, and s is the sign of σ. If $f(x)$ has a unique positive root, then $\Delta\phi$ is a uniquely defined number that imposes system charge neutrality. Since we are not aware of a general proof of this, we outline one.

Separating Eq. (8) into a sum of cation and anion terms, it can be generalized to

$$g(x) = \sum_{k=1}^{m} b_k x^k - \sum_{k=m+1}^{M} b_k x^k \tag{9}$$

with $b_k \geq 0$ [$b_k = |q_k|a_k$ (with $q_k = 0$ if that valence is not present) or $|s|$], m being the largest cation power of x in Eq. (8), and M being the largest anion power of x. If there is more than one positive root of $g(x)$, pick the two smallest at x_1 and x_2. Then, there must be a local minimum between them; at the smaller x_1, $g'(x_1) < 0$ because $g(0) > 0$ and $g(x_1) = 0$. Therefore, $g'(x_2) > 0$. In order for $g(x \to \infty) < 0$, there must be a maximum to the right of x_2. In other words, $g'(x)$ must have two positive roots. Playing the same game with g' and further derivatives, we eventually find a contradiction because $g^{(m+1)}(x) < 0$ for $x > 0$ and thus has no positive roots.

III. RESULTS

Since we study (negatively) charged confinement, one important output property is cation selectivity defined as

$$S_+ = \frac{\bar{N}_+ - \bar{N}_-}{\bar{N}_+ + \bar{N}_-}, \tag{10}$$

where $\bar{N}_i$ is the ensemble average of the total number of ionic species i in the confining geometry. The numerator is $-\sigma A/e$ for 1:1 electrolytes. For the 1:1 electrolyte studied here, $S_+ \sim 1$ is the perfectly cation selective case ($\bar{N}_- \sim 0$), while $S_+ \sim 0$ is the non-selective case ($\bar{N}_+ \sim \bar{N}_-$).

Since selectivity is a key factor in many applications from biology to energy conversion, we focus on the question of how we can attain better cation selectivity, or, put in a different way, better anion exclusion. It has been previously shown[51–53] that selectivity depends on the overlap of double layers, and, thus, it scales with λ_{D}/R in charged pores ($\lambda_{\text{D}} \propto c^{-1/2}$ is the Debye length). This means that we can increase selectivity either by decreasing c, or by decreasing R. Therefore, in this study, we only change the geometry radius R but not the reservoir concentration ($c_i^{\text{res}} = 0.1$). The pore radii used in this work ($R = 3$ and 5 nm) are larger than the ion radii ($R_i = 0.15$ nm), so volume exclusion effects (although interesting in other cases) are minimized here.

Figure 3 shows the number of particles normalized by the surface area [panel (a)] and by the volume [panel (b)] of the confining geometry as a function of ϵ^{sys}. Different colors indicate different geometries. Surface areas and volumes are $A = 2L^2$ and $V = 2RL^2$ for the slit, $A = 2R\pi L$ and $V = R^2\pi L$ for the pore, as well as $A = 4\pi R^2$ and $V = 4\pi R^3/3$ for the sphere, where L is the length of the simulation cell in the dimension in which it is homogeneous (not confined).

In Fig. 3(a), the difference between the cations and anions does not change because their difference is the surface charge density ($\sigma = -0.1e/\text{nm}^2$). As ϵ^{sys} decreases, the quantity of both species decreases due to the increasing solvation penalty [Eq. (7)]. The number of anions, however, approaches zero as $\epsilon^{\text{sys}} \to 40$. So, each geometry becomes more cation selective as ϵ^{sys} decreases because anions are excluded more. Meanwhile, the $\bar{N}_i/A$ values are smaller for more confined systems because there is less space for ions in such geometries.

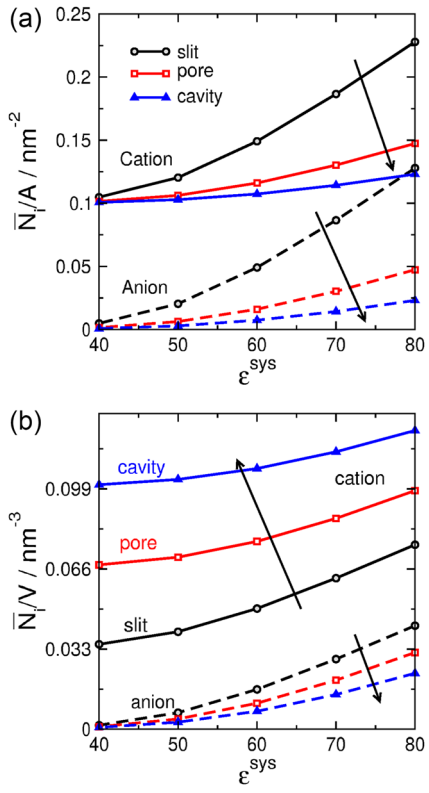

FIG. 3. Ensemble average of the total number of cations (solid line) and anions (dashed line) in confining geometries (indicated by colors) of radius $R = 3$ nm as a function of ϵ^{sys}. Panels (a) and (b) show the ion numbers normalized by the area, A, and the volume, V, of the confining geometry, respectively. The surface charge density is $\sigma = -0.1e/nm^2$. Here and in all the figures, $c_i^{res} = 0.1$ M. Arrows indicate the direction in which d_c increases.

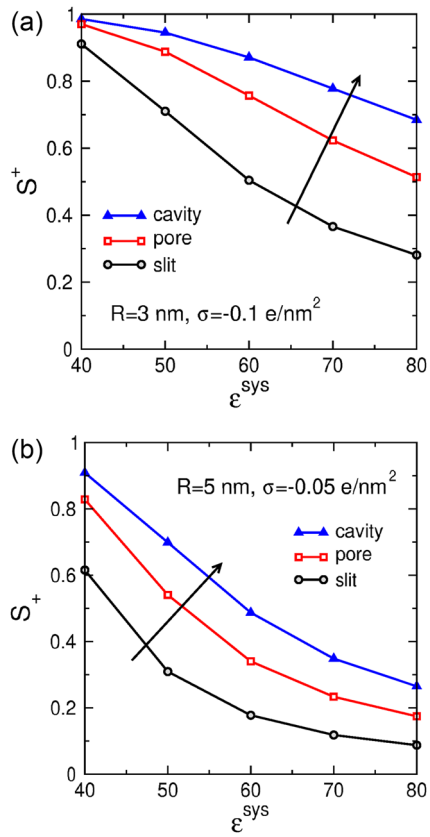

FIG. 4. Cation selectivities [Eq. (10)] as a function of the dielectric constant of the system, ϵ^{sys}, for different geometries (different colors). Panels (a) and (b) refer to different R and σ values, as indicated.

This is supported by Fig. 3(b), where we normalize with V. The average density of cations is larger in the systems with larger d_c. In the limiting case of perfect anion exclusion ($\epsilon^{sys} < 40$), the density of cations in the pore is twice that in the slit, and in the cavity, it is three times larger than in the slit (see more about this in Sec. IV).

While Fig. 3 characterizes the selectivity by showing normalized $\bar{N}_+$ and $\bar{N}_-$ values separately, it is also informative to describe various phenomena with just one number, the selectivity S_+. Therefore, in Fig. 4, we plot cation selectivity [Eq. (10)]. While Fig. 4(a) shows a more selective case (smaller R, larger $|\sigma|$), Fig. 4(b) shows a less selective case (larger R, smaller $|\sigma|$). The general behavior is that the selectivity for the more confined system is larger than for the less confined system; i.e., it is larger for the spherical cavity than for the cylindrical pore, for which it is larger than for the slit. Since the selectivity approaches 1 and 0 in the limiting cases of $\epsilon^{sys} \to 1$ and $\epsilon^{sys} \to \infty$, respectively, the curves imply a sigmoid-like form; the curves are concave down for large selectivities and concave up for small selectivities.

Figure 5 shows the concentration profiles that produce this behavior. Figure 5(a) shows the concentration curves with a linear scale, while Fig. 5(b) shows them with a logarithmic scale. Since the pore is strongly cation selective ($R = 1$ nm), the linear scale shows the behavior of the cations better, while the logarithmic scale shows the behavior of the anions better. Results for the various geometries (different line types) and for various dielectric constants (different colors) are shown.

Figure 5 shows that the number of confining dimensions has a large effect on the cation profiles. Cation concentrations are larger for the more confining geometries (slit < pore < cavity). As before, the cation concentration decreases with decreasing dielectric constant in all geometries due to the solvation penalty.

For anions, this dielectric effect is amplified: the dielectric constant has a larger effect on them than on the cations, at least, for the parameters used here (note that the same behavior is observed for $R = 3$ nm; see Fig. 3). Moreover, for a given ϵ^{sys}, anion exclusion is more effective as d_c increases; that is, anions are excluded from the cavity better than from the pore, and they are excluded from the pore better than from the slit.

In Fig. 6, we show the Donnan potential. It is always just a few kT/e, so its effect is generally mild. However, when this is combined with the differences in contact densities across various geometries [Fig. 5(a)], there may be additional changes in the surface charge in systems where there is charge regulation. This may have effects because pH-regulated surface charge, for instance, is sensitive to the local ion concentrations and electrostatic potential.[54]

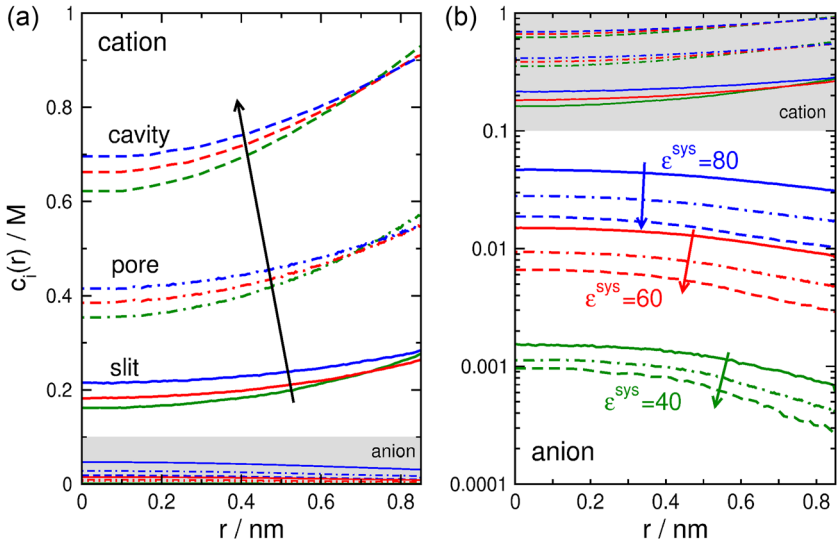

FIG. 5. Concentration profiles for different geometries (line styles) and dielectric constants (color). The left panel uses a linear scale for the ordinate, so it focuses on the cations, while the right panel uses a logarithmic scale for the ordinate, so it focuses on the anions. The curves below and above 0.1M refer to the anions and cations, respectively (see gray shading).

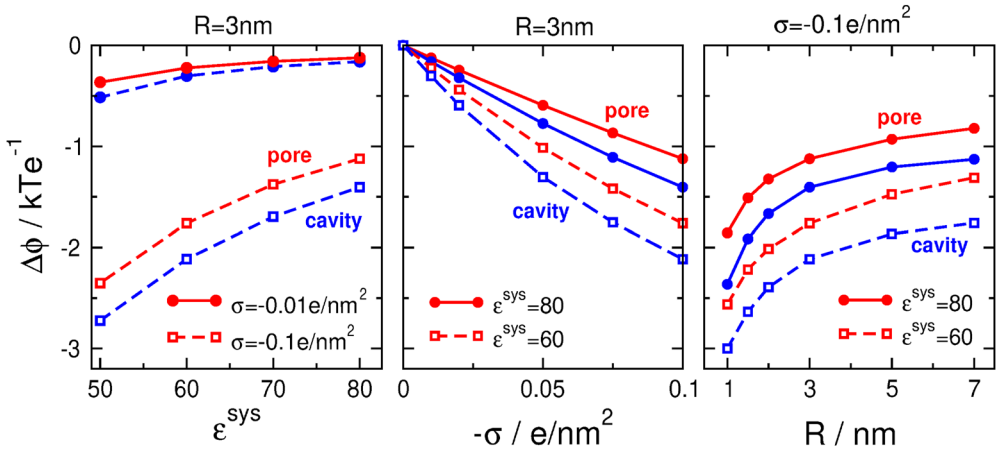

FIG. 6. Donnan potential as a function of ϵ^{sys} (left panel), $-\sigma$ (middle panel), and R (right panel) for various values of the other two parameters as indicated in the figure. Red and blue curves refer to the pore and cavity geometries, respectively. We only show $\Delta\phi$ for the pore and cavity because the simulation method used for the slit did not compute it directly; it uses moves of neutral ion groups (versus individual ion moves in the other geometries), which we have previously shown works equivalently but without explicitly referencing $\Delta\phi$.[38]

IV. DISCUSSION

Figure 5 shows a highly cation selective case, where the exclusion of the anions is especially efficient. The cation profiles show that the cation concentrations in the pore are approximately twice as large as in the slit and approximately three times larger in the cavity. The same behavior was noted in Fig. 3(b).

This finding can be understood by assuming that anion exclusion is perfect, so the surface charge, $|\sigma|A$, is neutralized only by the minimum number of cations, $\bar{c}_+ Ve$ (for monovalent cations), where A is the area of the confining surface, V is the volume of the confined region, and $\bar{c}_+$ is the average cation concentration (in the appropriate unit). Then, $|\sigma|A = \bar{c}_+ Ve$, and, therefore,

$$\bar{c}_+ = \frac{|\sigma|}{e}\frac{A}{V}. \tag{11}$$

Substituting A and V for the various geometries, we obtain that $\bar{c}_+$ is proportional to d_c,

$$\bar{c}_+ = \frac{|\sigma|}{e}\frac{d_c}{R}. \tag{12}$$

This simple derivation explains the behavior of the cation profiles in Fig. 5 and the average densities in Fig. 4(b). The problem could also be approached from the point of view of surface energetics and curvature.[55]

That the average counterion density and coion exclusion increases with increasing d_c is consistent with earlier studies.[39,41,42] The effect of decreasing ϵ^{sys} (dielectric exclusion) was also shown in many previous studies.[23–30,42] Here, we combined these two effects and showed that they mutually reinforce each other. By adding the varying dielectric constant to the change in the geometry, we gained

an additional system parameter with which partitioning of ions into a confined space can be optimized.

While we focused on the exclusion of coions in this study, it is relevant to note that the same principle can be used to distinguish the counterions of different charge (e.g., monovalent vs divalent) or different size. In GCMC studies for calcium channels, for example, it was proposed that Ca^{2+} ions are preferred over monovalent ions because they provide twice the charge to neutralize the negative charge of the pore modeled as a crowded region surrounded by a low-dielectric confinement.[48,56–58]

Multivalent electrolytes pose an especially interesting case, because the solvation penalty is four times larger for divalent ions, but the attraction of the negative charge of the pore is also stronger. This competition results in a diverse behavior that will be considered in subsequent studies.

The goal of this work was to define the physics of an idealized system where ions partition into confining low-dielectric environments. This foundation can then be built upon by adding layers of complexity to identify their individual effects in a controlled way. The next layers include adding solvent molecules, changing the homogeneous uniform surface charge distribution to more realistic localized ones,[59] and modeling hydrophobicity with a dielectric inhomogeneity, which is a computational challenge.[60]

ACKNOWLEDGMENTS

We acknowledge the financial support of the National Research, Development, and Innovation Office, under Grant Nos. NKFIH K137720 and TKP2021-NKTA-21. Research reported in this publication was supported by the National Heart, Lung, and Blood Institute of the National Institutes of Health under Award No. R01HL057832 to D.G.

AUTHOR DECLARATIONS

Conflict of Interest

The authors have no conflicts to disclose.

Author Contributions

János Szarvas: Data curation (equal); Formal analysis (equal); Investigation (equal); Validation (equal); Visualization (equal). **Mónika Valiskó**: Data curation (equal); Formal analysis (equal); Investigation (equal); Project administration (equal); Resources (equal); Validation (equal); Visualization (equal); Writing – review & editing (equal). **Dirk Gillespie**: Conceptualization (equal); Formal analysis (equal); Investigation (equal); Methodology (equal); Writing – review & editing (equal). **Dezső Boda**: Conceptualization (equal); Funding acquisition (equal); Investigation (equal); Methodology (equal); Project administration (equal); Resources (equal); Software (equal); Supervision (equal); Writing – original draft (equal).

DATA AVAILABILITY

The data that support the findings of this study are available from the corresponding author upon reasonable request.

REFERENCES

[1] P. Simon and Y. Gogotsi, Nat. Mater. **7**, 845 (2008).
[2] D. Gillespie, Nano Lett. **12**, 1410 (2012).
[3] M. A. Shannon, P. W. Bohn, M. Elimelech, J. G. Georgiadis, B. J. Mariñas, and A. M. Mayes, Nature **452**, 301 (2008).
[4] J. Cartailler, Z. Schuss, and D. Holcman, Physica D **339**, 39 (2017).
[5] W. Rocchia, E. Alexov, and B. Honig, J. Phys. Chem. B **105**, 6507 (2001).
[6] D. Boda, M. Valiskó, D. Henderson, D. Gillespie, B. Eisenberg, and M. K. Gilson, Biophys. J. **96**, 1293 (2009).
[7] K. Immadisetty, B. Sun, and P. M. Kekenes-Huskey, J. Phys. Chem. B **125**, 6390 (2021).
[8] W. Nonner, L. Catacuzzeno, and B. Eisenberg, Biophys. J. **79**, 1976 (2000).
[9] D. Boda, D. Henderson, and D. Gillespie, J. Chem. Phys. **139**, 055103 (2013).
[10] J. Barthel, R. Buchner, and M. Münsterer, *DECHEMA Chemistry Data Series* (DECHEMA, Frankfurt a.M, 1995), Vol. 12.
[11] M. Valiskó and D. Boda, Fluid Phase Equilib. **572**, 113826 (2023).
[12] H. Jäger, A. Schlaich, J. Yang, C. Lian, S. Kondrat, and C. Holm, Faraday Discuss. **246**, 520–539 (2023).
[13] L. Bocquet and E. Charlaix, Chem. Soc. Rev. **39**, 1073 (2010).
[14] N. Kavokine, R. R. Netz, and L. Bocquet, Annu. Rev. Fluid. Mech. **53**, 377 (2021).
[15] D. Muñoz-Santiburcio and D. Marx, Chem. Rev. **121**, 6293 (2021).
[16] L. Fumagalli, A. Esfandiar, R. Fabregas, S. Hu, P. Ares, A. Janardanan, Q. Yang, B. Radha, T. Taniguchi, K. Watanabe, G. Gomila, K. S. Novoselov, and A. K. Geim, Science **360**, 1339–1342 (2018).
[17] P. Loche, C. Ayaz, A. Wolde-Kidan, A. Schlaich, and R. R. Netz, J. Phys. Chem. B **124**, 4365–4371 (2020).
[18] S. Senapati and A. Chandra, J. Phys. Chem. B **105**, 5106–5109 (2001).
[19] D. J. Bonthuis, S. Gekle, and R. R. Netz, Phys. Rev. Lett. **107**, 166102 (2011).
[20] K. Vasanth Kumar and F. Rodríguez-Reinoso, Nanotechnology **24**, 035401 (2012).
[21] N. Song, T. Kakuta, T.-A. Yamagishi, Y.-W. Yang, and T. Ogoshi, Chem **4**, 2029–2053 (2018).
[22] H. Zhu and B. Hu, Membranes **12**, 220 (2022).
[23] H. Zhang and G. M. Geise, J. Membr. Sci. **520**, 790–800 (2016).
[24] A. Yaroshchuk, M. L. Bruening, and E. Zholkovskiy, Adv. Colloid Interface Sci. **268**, 39–63 (2019).
[25] K. Chang, H. Luo, and G. M. Geise, J. Membr. Sci. **574**, 24–32 (2019).
[26] A. E. Yaroshchuk, Adv. Colloid Interface Sci. **85**, 193–230 (2000).
[27] E. S. Zofchak, Z. Zhang, N. Marioni, T. J. Duncan, H. S. Sachar, A. Chamseddine, B. D. Freeman, and V. Ganesan, Macromolecules **55**, 2260–2270 (2022).
[28] V. Freger, Adv. Colloid Interface Sci. **319**, 102972 (2023).
[29] S. M. Bannon and G. M. Geise, ACS Macro Lett. **13**, 515–520 (2024).
[30] S. M. Bannon and G. M. Geise, J. Membr. Sci. **694**, 122396 (2024).
[31] J. Mittal and R. B. Best, Proc. Natl. Acad. Sci. U. S. A. **105**, 20233–20238 (2008).
[32] R. J. Tomlin, T. Roy, T. L. Kirk, M. Marinescu, and D. Gillespie, J. Electrochem. Soc. **169**, 120513 (2022).
[33] L. Lue and P. Linse, J. Chem. Phys. **142**, 144902 (2015).
[34] G. Chen, J. Micromech. Mol. Phys. **7**, 127–134 (2022).
[35] R. Wang, P. Biesheuvel, and M. Elimelech, J. Membr. Sci. **705**, 122921 (2024).
[36] S. A. Barr and A. Z. Panagiotopoulos, Phys. Rev. E **86**, 016703 (2012).
[37] J. Landsgesell, P. Hebbeker, O. Rud, R. Lunkad, P. Košovan, and C. Holm, Macromolecules **53**, 3007 (2020).
[38] D. Boda and D. Gillespie, J. Mol. Liq. **391**, 123372 (2023).
[39] E. Sánchez-Arellano, W. Olivares, M. Lozada-Cassou, and F. Jiménez-Ángeles, J. Colloid Interface Sci. **330**, 474–482 (2009).
[40] G. E. Aguilar-Pineda, F. Jiménez-Ángeles, J. Yu, and M. Lozada-Cassou, J. Phys. Chem. B **111**, 2033–2044 (2007).
[41] A. G. Cherstvy, Biopolymers **97**, 311–317 (2012).
[42] A. Szymczyk and P. Fievet, J. Membr. Sci. **252**, 77–88 (2005).
[43] S. Buyukdagli, M. Manghi, and J. Palmeri, Phys. Rev. Lett. **105**, 158103 (2010).
[44] S. Buyukdagli, M. Manghi, and J. Palmeri, J. Chem. Phys. **134**, 074706 (2011).

[45]T. Hennequin, M. Manghi, and J. Palmeri, Phys. Rev. E **104**, 044601 (2021).
[46]A. Malasics and D. Boda, J. Chem. Phys. **132**, 244103 (2010).
[47]M. Born, Z. Phys. **1**, 45 (1920).
[48]D. Boda, M. Valiskó, B. Eisenberg, W. Nonner, D. Henderson, and D. Gillespie, J. Chem. Phys. **125**, 034901 (2006).
[49]D. Boda, D. Henderson, B. Eisenberg, and D. Gillespie, J. Chem. Phys. **135**, 064105 (2011).
[50]D. Gillespie and R. S. Eisenberg, Phys. Rev. E **63**, 061902 (2001).
[51]Z. Sarkadi, D. Fertig, Z. Ható, M. Valiskó, and D. Boda, J. Chem. Phys. **154**, 154704 (2021).
[52]Z. Sarkadi, D. Fertig, M. Valiskó, and D. Boda, J. Mol. Liq. **357**, 119072 (2022).
[53]Z. Sarkadi, Z. Ható, M. Valiskó, and D. Boda, J. Mol. Liq. **387**, 122571 (2023).
[54]A. Eden and S. Pennathur, Adv. Mater. Interfaces 2400495 (published online).
[55]J. Groenewold, J. Chem. Phys. **107**, 9668–9676 (1997).
[56]D. Boda, M. Valiskó, B. Eisenberg, W. Nonner, D. Henderson, and D. Gillespie, Phys. Rev. Lett. **98**, 168102 (2007).
[57]D. Gillespie and D. Boda, Biophys. J. **95**, 2658 (2008).
[58]D. Boda, M. Valiskó, D. Henderson, B. Eisenberg, D. Gillespie, and W. Nonner, J. Gen. Physiol. **133**, 497 (2009).
[59]H. Fábián, Z. Sarkadi, M. Valiskó, D. Gillespie, and D. Boda, J. Mol. Liq. **368**, 120715 (2022).
[60]D. Boda, D. Gillespie, W. Nonner, D. Henderson, and B. Eisenberg, Phys. Rev. E **69**, 046702 (2004).